CONSTRAINTS ON THE ENVIRONMENT AND ENERGETICS OF THE BROAD-LINE IC SN 2014AD FROM DEEP RADIO AND X-RAY OBSERVATIONS

M. MARONGIU[1,2], C. GUIDORZI[1], R. MARGUTTI[3], D. L. COPPEJANS[3], R. MARTONE[1,2], A. KAMBLE[4]
Draft version May 30, 2019

ABSTRACT

Broad-line type Ic Supernovae (BL-Ic SNe) are characterized by high ejecta velocity ($\gtrsim 10^4$ km s^{-1}) and are sometimes associated with the relativistic jets typical of long duration ($\gtrsim 2$ s) Gamma-Ray Bursts (L-GRBs). The reason why a small fraction of BL-Ic SNe harbor relativistic jets is not known. Here we present deep X-ray and radio observations of the BL-Ic SN 2014ad extending from 13 to 930 days post explosion. SN 2014ad was not detected at either frequency and has no observational evidence of a GRB counterpart. The proximity of SN 2014ad ($d \sim 26$ Mpc) enables very deep constraints on the progenitor mass-loss rate $\dot{M}$ and on the total energy of the fast ejecta E. We consider two synchrotron emission scenarios for a wind-like circumstellar medium (CSM): (i) uncollimated non-relativistic ejecta, and (ii) off-axis relativistic jet. Within the first scenario our observations are consistent with GRB-less BL-Ic SNe characterized by a modest energy budget of their fast ejecta ($E \lesssim 10^{45}$ erg), like SNe 2002ap and 2010ay. For jetted explosions, we cannot rule out a GRB with $E \lesssim 10^{51}$ erg (beam-corrected) with a narrow opening angle ($\theta_j \sim 5°$) observed moderately off-axis ($\theta_{\rm obs} \gtrsim 30°$) and expanding in a very low CSM density ($\dot{M} \lesssim 10^{-6}$ M$_\odot$ yr^{-1}). Our study shows that off-axis low-energy jets expanding in a low-density medium cannot be ruled out even in the most nearby BL-Ic SNe with extensive deep observations, and might be a common feature of BL-Ic SNe.

Subject headings: techniques: interferometric radio analysis - gamma-ray burst: general - supernovae: general - supernovae: individual: 2014ad

1. INTRODUCTION

Type Ic supernovae (SNe) are hydrogen-stripped core-collapse explosions (CCSNe) of massive stars with $M_{ZAMS} \gtrsim 8 M_\odot$ that show no evidence for hydrogen and helium in their spectra (Filippenko 1997). Potential candidates for type Ic SN progenitors are massive Wolf Rayet (WR) stars and stars in close binary systems (Ensman & Woosley 1988; Gal-Yam 2017). At the time of writing the exact nature of their progenitors is unclear (Podsiadlowski et al. 1992; Yoon 2010; Eldridge et al. 2013; Smartt 2009, 2015; Dessart 2015; Dessart et al. 2015, 2017). Notable in this respect is the recent detection of the progenitor system of the Ic SN 2017ein (Kilpatrick et al. 2018; Van Dyk et al. 2018) which pointed to a massive stellar progenitor with $M \sim 60 M_\odot$ in a binary system.

Ic SNe typically show a bell-shaped radio spectrum powered by synchrotron emission and extending all the way to the X-ray band. The spectral peak frequency describes the transition between the optically thick part of the spectrum –below which synchrotron self-absorption (SSA) takes place– and the optically thin portion of the spectrum (Rybicki & Lightman 1979; Chevalier 1998; Chevalier & Fransson 2006). The synchrotron emission is produced by electrons that are accelerated at the shock front between the SN ejecta and the the circumstellar medium (CSM). As the shock wave expands, the optical depth to SSA decreases and hence the spectral peak

frequency cascades down to lower frequencies with time. In a SN explosion, the X-ray and radio emission resulting from the SN shock propagation in the medium track the fastest material ejected by the explosion, while the optical emission is of thermal origin and originates from the inner ejecta layers.

A small fraction ($\sim 4\%$; Shivvers et al. 2017) of Ic SNe, called broad-line Ic SNe (BL-Ic SNe), are characterized by broad lines in the optical spectrum implying large expansion velocities of the ejecta ($\gtrsim 2 \times 10^4$ km s^{-1}, e.g. Mazzali et al. 2002; Cano et al. 2017), $\sim 10^4$ km s^{-1} faster than in "ordinary" Ic SNe (Modjaz et al. 2016). Some BL-Ic SNe are associated with ultra-relativistic jets that generate long duration ($\gtrsim 2$ s) Gamma-Ray Bursts (L-GRBs, e.g. Cano et al. 2017), which are observable at cosmological distances up to $z \sim 10$ (e.g. Cucchiara et al. 2011). In the local universe ($z \leq 0.1$) some BL-Ic SNe have also been found in association with mildly relativistic outflows in low-luminosity GRBs (ll-GRBs, which are too weak to be detected at larger distances, Liang et al. 2007). As opposed to L-GRBs, ll-GRBs show no evidence for collimation of their fastest ejecta, i.e. no jet (Kulkarni et al. 1998; Soderberg et al. 2006b; Bromberg et al. 2011).

A possible interpretation of the observational lack of evidence for L-GRB counterparts in the majority of BL-Ic SNe is the off-axis jet scenario (Rhoads 1999; Eichler & Levinson 1999; Yamazaki et al. 2003; Piran 2004; Soderberg et al. 2006a; Bietenholz 2014; Corsi et al. 2016), where the explosion powers a GRB-like jet that is misaligned with respect to the observer line of sight. In this scenario, as the jet velocity gradually decreases and relativistic beaming becomes less severe, the emission becomes observable from increasingly larger viewing angles. Deep radio and X-ray observations extending to hundreds of days post explosion offer the opportunity to reveal the emission from off-axis jets as well as to recover weak GRBs that would not trigger current γ-ray

marco.marongiu@unife.it

[1] Department of Physics and Earth Science, University of Ferrara, via Saragat 1, I–44122, Ferrara, Italy

[2] ICRANet, Piazzale della Repubblica 10, 65122, Pescara, Italy

[3] Center for Interdisciplinary Exploration and Research in Astrophysics (CIERA) and Department of Physics and Astronomy, Northwestern University, Evanston, IL 60208, USA

[4] formerly at Harvard-Smithsonian Center for Astrophysics, 60 Garden St. Cambridge. MA 02138, USA

observing facilities.

Here we present extensive ($\delta t \sim 10 - 1000$ days) broadband (radio to X-ray) observations of SN 2014ad, a BL-Ic SN that exploded in the galaxy PGC 37625 (Mrk 1309) at $d = 26.44$ Mpc (Sahu et al. 2018). SN 2014ad is among the closest BL-Ic SNe discovered to date, which enables very deep limits on its radio and X-ray emission (Figure 1 and Table 1). We present constraints on the progenitor mass-loss rate $\dot{M}$ and the total energy of the fast ejecta E in two scenarios: (i) mildly relativistic, nearly isotropic, synchrotron self-absorbed radio emission due to the SN ejecta ploughing through a wind-like CSM; (ii) synchrotron emission from a relativistic off-axis GRB-like jet.

The analysis of the optical emission from SN 2014ad by Sahu et al. (2018) and Stevance et al. (2017) revealed that the bulk of its ejecta velocity is $\sim 3 \times 10^4$ km s^{-1} at early times, with kinetic energy $E_k \sim (1.0 \pm 0.3) \times 10^{52}$ erg, larger than in type-Ic SNe, and similar to BL-Ic SNe and GRB-SNe. The metallicity of the host galaxy of SN 2014ad is ~ 0.5 Z$_\odot$. The total explosion ejecta mass inferred by Sahu et al. (2018) and Stevance et al. (2017) is $M_{ej} \sim (3.3 \pm 0.8)$ M$_\odot$ suggesting a massive progenitor star with $M_{ZAMS} \gtrsim 20$ M$_\odot$. Spectropolarimetry by Stevance et al. (2017) also suggests a mild deviation from a spherical geometry of the ejecta.

This paper is organized as follows. In Section 2 we describe our radio and X–ray observations; in Section 3 we present the constraints on the environment derived from our X-ray limits, whereas in Section 4 we present environment constraints derived from the radio and X-ray broadband modeling in two different scenarios (i.e., an "ordinary" isotropic SN outflow, and a beamed relativistic jet). Our results and analysis are discussed in Section 5 and conclusions are drawn in Section 6.

2. OBSERVATIONS

SN 2014ad was discovered by Howerton et al. (2014) on March 12.4, 2014 (MJD 56728.4) in public images from the Catalina Real-Time Transient Survey (Djorgovski et al. 2011) at $\alpha = 11^h57^m44^s.44$, $\delta = -10°10'15.7''$. Throughout this paper we assume a SN explosion date $t_0 = 56725 \pm 3$ MJD (Sahu et al. 2018); times given are in reference to this explosion date unless otherwise noted.

2.1. Radio Observations with the VLA

VLA follow-up observations were carried out between March 22, 2014 (MJD 56738) and September 23, 2016 (MJD 57654), from ~ 13 d to ~ 930 d post explosion, under Proposal VLA/14A-531 (PI: Kamble). Data were taken in eight spectral windows at L-band (with baseband central frequencies of 1.3 and 1.7 GHz, respectively), C-band (5 and 7 GHz), X-band (8.5 and 11 GHz), Ku-band (13.5 and 16 GHz), with a nominal bandwidth of ~ 1 GHz (~ 0.4 GHz for L-band). 3C286 and J1330-1449 were used as flux/bandpass and phase/amplitude calibrators, respectively. The Common Astronomy Software Application (CASA, v. 4.7.2, McMullin et al. 2007)[5] was used to calibrate, flag and image the data. Images were formed from the visibility data using the CLEAN algorithm (Högbom 1974). The image size was set to (1024 × 1024) pixels, the pixel size was determined as 1/5 of the nominal beam width and the images were cleaned using natural weighting. The upper limits on the flux densities were calculated at a 3σ confidence level (Table 1).
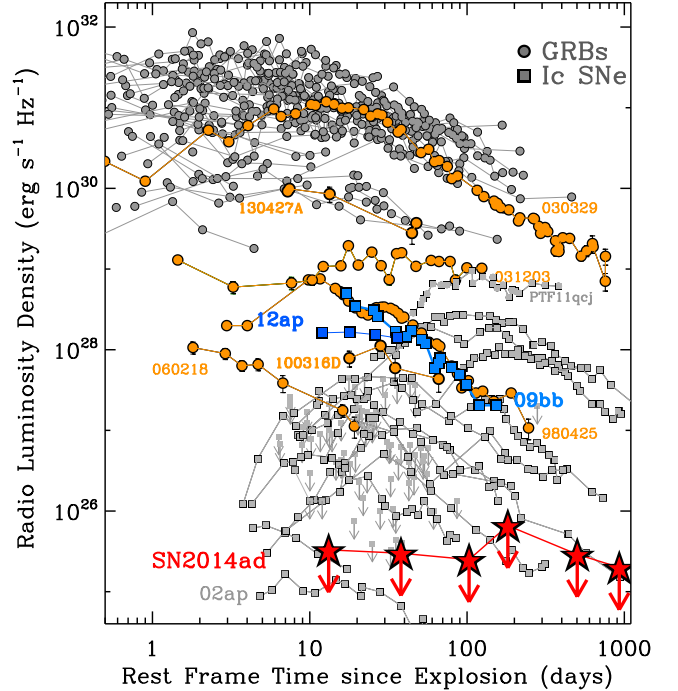
FIG. 1.— Deep radio limits on the emission from SN 2014ad (red stars) in the context of L-GRBs (circles; gray is for cosmological GRBs, while orange is for GRBs at $z \leq 0.3$) and H-stripped CCSNe (squares; gray is for normal SNe, blue is for SNe with relativistic ejecta). Our deep radio limits on the emission from the BL-Ic SN 2014ad are consistent with a luminosity comparable to that of SN 2002ap. The detected radio emission from SN 2002ap points to a non-relativistic (shock velocity $\sim 0.3c$) uncollimated explosion with a small energy budget of the fast ejecta ($E \sim 1.5 \times 10^{45}$ erg; Berger et al. 2002).

2.2. X–ray Observations with Swift-XRT

The X-Ray Telescope (XRT; Burrows et al. 2005) onboard the *Swift* Gehrels spacecraft (Gehrels et al. 2004) observed the region of SN 2014ad in Photon Counting (PC) mode several times from March 19, 2014 to March 11, 2017. We find no evidence for statistically significant X-ray emission at the location of SN 2014ad. We extracted the 0.3–10 keV light curve, consisting of 3σ upper limits, using the web interface provided by Leicester University[6], which used HEASOFT (v. 6.22). We performed flux calibration by assuming an absorbed simple power-law spectral model (WABS*POWERLAW within XSPEC) with column density frozen to the Galactic value along the SN line of sight, $N_{H,Gal} = 3.1 \times 10^{20}$ cm^{-2} (Kalberla et al. 2005). We assumed a conservative value for the photon index, $\Gamma = 2$, and derived the upper limit to the flux density at 1 keV. Finally, we calculated three light curves with different integration times: 10^5, 2×10^5, and 5×10^5 s, respectively. Table 2 reports the values for the longest timescale having the deepest limits. We also calculated the corresponding 3σ upper limits on the 0.3–10 keV luminosity.

3. CONSTRAINTS ON THE ENVIRONMENT DENSITY FROM INVERSE COMPTON EMISSION

Inverse Compton (IC) emission from the upscattering of optical photospheric photons into the X-ray band by relativistic electrons at the shock front has been demonstrated to dominate the X-ray emission from H-stripped CCSNe that explode

TABLE 1
LOG OF VLA OBSERVATIONS OF SN 2014AD: OBSERVATION CENTRAL TIME t_{mid}, EPOCH
$t_e = t_{mid} - t_0$ SINCE THE ESTIMATED EXPLOSION DATE t_0, VLA ARRAY CONFIGURATION, BEAM SIZE
θ_{FWHM}, CENTRAL FREQUENCY ν_c AND ITS BANDWIDTH $\Delta\nu$, THE UNCERTAINTY σ_S, THE UPPER
LIMIT ON THE FLUX DENSITY S (AT 3$-\sigma$) AND THE RELATIVE LUMINOSITY L_{25} (IN UNITS OF 10^{25}
ERG S^{-1} HZ^{-1}) OF THE SOURCE. IN NO CASE WAS THE SOURCE WAS DETECTED WITH $\geq 3-\sigma$
CONFIDENCE.

t_{mid} [MJD]	t_e [days]	VLA Configuration	θ_{FWHM} [arcsec]	ν_c [GHz]	$\Delta\nu$ [GHz]	σ_S [μJy]	S(3$-\sigma$) [μJy]	L_{25} [erg s^{-1} Hz^{-1}]
56738.19	13.19	A	1.42	1.26	0.384	28.8	86.4	12.1
		A	0.93	1.80	0.384	30.8	92.4	12.9
		A	0.34	5.0	0.896	9.0	27.0	3.8
		A	0.24	7.1	0.896	8.1	24.3	3.4
		A	0.19	8.6	0.896	7.9	20.7	3.3
		A	0.15	11.0	0.896	7.8	23.4	3.3
		A	0.13	13.5	0.896	7.7	23.1	3.2
		A	0.11	16.0	0.896	9.1	27.3	3.8
56763.21	38.21	A	1.42	1.26	0.384	31.6	94.8	13.2
		A	0.93	1.80	0.384	31.4	94.2	13.1
		A	0.34	5.0	0.896	10.5	31.5	4.4
		A	0.24	7.1	0.896	7.2	21.6	3.0
		A	0.19	8.6	0.896	8.0	24.0	3.4
		A	0.15	11.0	0.896	10.3	30.9	4.3
		A	0.13	13.5	0.896	7.3	21.9	3.1
		A	0.11	16.0	0.896	7.6	22.8	3.2
56828.96	103.96	AnD	12.02	5.0	0.896	6.9	20.7	2.9
		AnD	7.93	7.1	0.896	5.2	15.6	2.2
		AnD	0.20	8.6	0.896	6.0	18.0	2.5
		AnD	0.15	11.0	0.896	6.3	18.9	2.6
56906.76	181.76	D	12.02	5.0	0.896	13.9	41.7	5.8
		D	7.93	7.1	0.896	10.8	32.4	4.5
		D	6.98	8.6	0.896	15.7	47.1	6.6
		D	5.46	11.0	0.896	16.8	50.4	7.0
57227.81	502.81	A	0.34	5.0	0.896	9.9	26.7	4.1
		A	0.24	7.1	0.896	9.4	27.7	3.9
		A	0.19	8.6	0.896	6.9	20.7	2.9
		A	0.15	11.0	0.896	10.1	30.3	4.2
57654.66	929.66	B	1.15	5.0	0.896	6.6	19.8	2.8
		B	0.79	7.1	0.896	6.3	18.9	2.6
		B	0.65	8.6	0.896	7.0	21.0	2.9
		B	0.51	11.0	0.896	6.8	20.4	2.8

TABLE 2
Swift-XRT 3$-\sigma$ UPPER LIMITS ON THE FLUX DENSITY AT
1 KEV ($F_{\nu, 1\,KeV}$) AND 0.3–10 KEV LUMINOSITY ($L_{0.3-10}$).
$t_e = t_{mid} - t_0$ IS THE EPOCH SINCE THE ESTIMATED SN
EXPLOSION DATE t_0, Δt IS THE BIN TIME.

t_{mid} [MJD]	t_e [days]	Δt [days]	$F_{\nu, 1\,KeV}$ [μJy]	$L_{0.3-10}$ [erg s^{-1}]
56738.1	13.1	5.8	$< 1.3 \times 10^{-2}$	$< 1.0 \times 10^{42}$
56743.9	18.9	5.8	$< 1.2 \times 10^{-2}$	$< 9.0 \times 10^{41}$
56749.6	24.6	5.8	$< 1.7 \times 10^{-2}$	$< 1.3 \times 10^{42}$
56755.4	30.4	5.8	$< 4.1 \times 10^{-2}$	$< 3.2 \times 10^{42}$
57774.0	1049.0	5.8	< 0.11	$< 8.5 \times 10^{42}$
57808.7	1083.7	5.8	< 1.1	$< 8.5 \times 10^{43}$
57820.2	1095.2	5.8	$< 6.7 \times 10^{-2}$	$< 5.2 \times 10^{42}$

in low-density environments ($\dot{M} \lesssim 10^{-5}$ M$_\odot$ yr^{-1}) at $\delta t \lesssim$ 30 d (e.g. Björnsson & Fransson 2004; Chevalier & Fransson 2006). We adopt the IC formalism by Margutti et al. (2012) modified to account for the outer density structure of progenitors of BL-Ic SNe (which are likely to be compact) as in Margutti et al. (2014). The IC emission depends on: (i) the density structure of the SN ejecta and of the CSM; (ii) the electron distribution responsible for the up-scattering; (iii) explosion parameters (ejecta mass M_{ej} and kinetic energy[7] E_k);

[7] This is the kinetic energy carried by the slowly moving material powering the optical emission.

and (iv) the bolometric luminosity of the SN: $L_{IC} \propto L_{bol}$.

For compact progenitors that are relevant here, the density scales as $\rho_{SN} \propto r^{-n}$ with $n \sim 10$ (see e.g. Matzner & McKee 1999; Chevalier & Fransson 2006). We further assume a power-law electron distribution $n_e(\gamma) \propto \gamma^{-p}$ with $p \sim 3$ as found in radio observations of type H-stripped CCSNe (Chevalier & Fransson 2006) and a fraction of energy into relativistic electrons $\epsilon_e = 0.1$. We use the explosion parameters $E_k = (1 \pm 0.3) \times 10^{52}$ erg and $M_{ej} = (3.3 \pm 0.8)$ M$_\odot$. For a wind-like CSM structure $\rho_{CSM} \propto r^{-2}$ with a typical wind velocity $v_w = 1000$ km s^{-1} as appropriate for massive stars (and hence BL-Ic SN progenitors, e.g. Smith 2014), the *Swift*-XRT non-detections at $\delta t < 30$ d yield $\dot{M} < 5 \times 10^{-5}$ M$_\odot$ yr^{-1}.

4. BROADBAND MODELING

We interpret our deep radio and X-ray limits in the context of synchrotron self-absorbed (SSA) emission from either (i) uncollimated (i.e. spherical) non-relativistic ejecta (Sect. 4.1), or (ii) relativistic GRB-like jet (Sect. 4.2).

4.1. *SSA emission from non-relativistic uncollimated ejecta*

We follow Soderberg et al. (2005) and adopt their formalism in the context of the radio emission from non-relativistic SN ejecta interacting with a wind-like CSM. The brightness temperature of a source is:

$$T_B = \frac{c^2}{2\pi k} \frac{f_\nu d^2}{(v_{ph}t)^2 \nu^2} ,\qquad (1)$$

where c is the speed of light, k is the Boltzmann constant, f_ν is the flux density at observed frequency ν, d is the source distance, v_{ph} is the photospheric velocity and t is the observational epoch. For SN 2014ad we find $T_B \lesssim 2.8 \times 10^{11}$ K at $t \sim 13.2$ d, where $v_{ph} \sim 3.2 \times 10^4$ km s^{-1} and $f_\nu < 86.4$ μJy at $\nu = 1.26$ GHz (Table 1). Our inferred T_B does not violate the 10^{12} K limit of the Inverse Compton Catastrophe (ICC; Kellermann & Pauliny-Toth 1981), consistent with the expectations from a non relativistic spherical SSA source.

In the SSA model radiation originates from an expanding spherical shell of shock-accelerated electrons with radius r and thickness r/η (here we assume the standard scenario of a thin shell with $\eta = 10$; e.g. Li & Chevalier 1999; Soderberg et al. 2005). As the shock wave propagates through the CSM, it accelerates relativistic electrons into a power-law distribution $N(\gamma) \propto \gamma^{-p}$ for $\gamma \geq \gamma_m$, where γ_m is the minimum Lorentz factor of the electrons (Chevalier 1982, 1998). In this analysis we assume $p \sim 3$ as typically found in H-stripped core-collapse SNe (e.g. Chevalier & Fransson 2006). The post-shock energy fraction in the electrons and magnetic field is given by ϵ_e and ϵ_B, respectively; we further adopt equipartition of the post-shock energy density of the radio-emitting material between relativistic electrons and magnetic fields ($\epsilon_e = \epsilon_B = 1/3$).

The synchrotron emission from SNe typically peaks at radio frequencies on timescales of a few days to weeks after the SN explosion (e.g. Corsi et al. 2014); this emission is suppressed at low frequencies by absorption processes. Chevalier (1998) showed that the dominant absorption process is internal SSA for H-stripped SNe, and external free-free absorption (FFA) in H-rich SNe, as H-rich SNe tend to explode in higher density media.

Following Soderberg et al. (2005), the temporal evolution of the magnetic field $B(t)$, minimum Lorentz factor $\gamma_m(t)$, shock radius $r(t)$ and the ratio $\Im = \epsilon_e/\epsilon_B$) can be parametrized as:

$$B = B_0 \left(\frac{t-t_e}{t_0-t_e}\right)^{\alpha_B} \qquad \gamma_m = \gamma_{m,0} \left(\frac{t-t_e}{t_0-t_e}\right)^{\alpha_\gamma} \quad (2)$$

$$r = r_0 \left(\frac{t-t_e}{t_0-t_e}\right)^{\alpha_r} \qquad \Im = \Im_0 \left(\frac{t-t_e}{t_0-t_e}\right)^{\alpha_\Im} \quad (3)$$

where r_0, B_0, $\Im_0$ and $\gamma_{m,0}$ are measured at an arbitrary reference epoch t_0, and t_e is the explosion time. In this paper we adopt $t_0 = 13.2$ d (for which $r_0 \sim v_{ph} \times t_0 = 4 \times 10^{15}$ cm) and $t_e = 0$ d. The temporal indices α_r, α_B, $\alpha_\Im$, α_γ are determined by the hydrodynamic evolution of the ejecta, as described in Soderberg et al. (2005). In particular, α_r and $\alpha_\Im$ can be expressed as:

$$\alpha_r = \frac{n-3}{n-s}, \quad (4)$$

$$\alpha_\Im = -s\alpha_r + \alpha_\gamma - 2\alpha_B, \quad (5)$$

where n and s describe the density profile of the outer SN ejecta ($\rho_{ej} \propto r^{-n}$), and of the CSM ($\rho_{CSM} \propto r^{-s}$)[8], respectively. The self-similar conditions $s < 3$ and $n > 5$ result in $\sim 0.5 < \alpha_r < 1$ (Chevalier 1982). In this work we consider a wind-like CSM case (i.e. $s = 2$), and $n = 10$ as appropriate for massive compact stars that are thought to be progenitors of H-stripped CCSNe. In the standard scenario (Chevalier 1996), ϵ_e and ϵ_B

do not vary with time, from which we derive through Eq. 3 that $\alpha_\Im = 0$, implying that:

$$\alpha_B = \left(\frac{2-s}{2}\right)\alpha_r - 1, \quad (6)$$

$$\alpha_\gamma = 2(\alpha_r - 1). \quad (7)$$

Since $\alpha_\Im = 0$ and under the equipartition hypothesis ($\Im = 1$; Eq. 3), it follows that $\alpha_r = 0.875$ (Eq. 4), $\alpha_B = -1$ (Eq. 6) and $\alpha_\gamma = -0.25$ (Eq. 7).

Under these assumptions and through Eq. (2), the characteristic synchrotron frequency is:

$$\nu_m(t) = \gamma_m^2 \frac{qB}{2\pi m_e c} = \gamma_{m,0}^2 \frac{qB_0}{2\pi m_e c} \left(\frac{t}{t_0}\right)^{2\alpha_\gamma + \alpha_B}$$
$$= \nu_{m,0} \left(\frac{t}{t_0}\right)^{2\alpha_\gamma + \alpha_B}, \quad (8)$$

where q is the electron charge and m_e is the electron mass. The frequency $\nu_{m,0} \equiv \nu_m(t_0)$ depends on $\gamma_{m,0}$ and B_0 as follows:

$$\nu_{m,0} = \gamma_{m,0}^2 \frac{qB_0}{2\pi m_e c}. \quad (9)$$

The radio flux density at a given observing frequency ν and epoch t is thus given by:

$$F(t,\nu) = 10^{26} C_f \left(\frac{t}{t_0}\right)^{(4\alpha_r - \alpha_B)/2} \left(1 - e^{-\tau_\nu^\xi}\right)^{1/\xi}$$
$$\times \nu^{5/2} F_3(x) F_2^{-1}(x) \quad \text{mJy} \quad (10)$$

with the optical depth τ_ν:

$$\tau_\nu(t) = C_\tau \left(\frac{t}{t_0}\right)^{\alpha_r + (3+p/2)\alpha_B + (p-2)\alpha_\gamma + \alpha_\Im} \nu^{-(p+4)/2} F_2(x). \quad (11)$$

C_f and C_τ are normalization constants (see Appendix A2 of Soderberg et al. 2005), $F_2(x)$ and $F_3(x)$ are Bessel functions with $x = 2/3 (\nu/\nu_m)$, $\xi = [0, 1]$ describes the sharpness of the spectral break between optically thin and thick regimes. We adopt $\xi = 1$.

As we can see from Eqs (10, 11, 4 and 8), $F(t,\nu)$ depends on C_f, C_τ, p, n, s, $\nu_{m,0}$, and ξ. From Eqs 6–8 of Soderberg et al. (2005) C_f and C_τ can be expressed in terms of r_0, B_0 and η; thus, also using (9), $F(t,\nu)$ can be expressed as a function of r_0, B_0, p, n, s, $\gamma_{m,0}$, η, and ξ, which are all fixed apart from B_0 and $\gamma_{m,0}$. These two free parameters can be further expressed as a function of physically more useful quantities[9], the SN progenitor mass-loss rate ($\dot{M}$) and the total kinetic energy of the radio-bright (fast) ejecta (E):

$$B_0 = \left(\frac{2\eta\epsilon_e}{\Im_0 r_0^3}\right)^{1/2} E^{1/2} \quad (12)$$

$$\gamma_{m,0} = \left(\frac{p-2}{p-1}\right) \frac{2m_p \epsilon_e v_w}{m_e c^2 r_0} \left(\frac{E}{\dot{M}}\right) \quad (13)$$

where m_p is the proton mass and v_w is the wind velocity. Con-

---

[8] $s = 0$ corresponds to the case of ISM-like CSM and $s = 2$ correspond to the case of wind-like CSM.

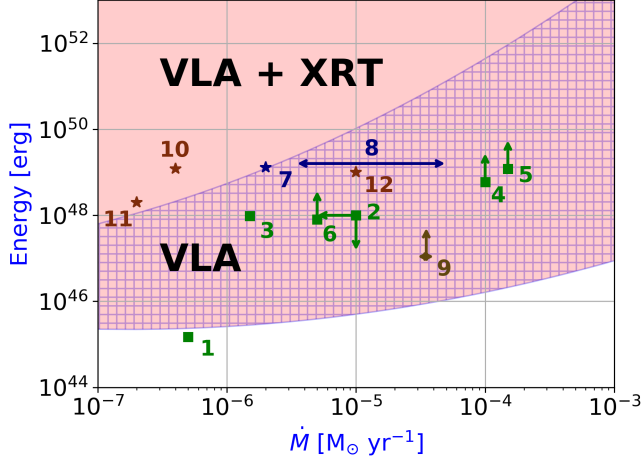[9] These parameters are showed in Eqs. 13 and 14 of Soderberg et al. (2005), respectively.

FIG. 2.— Regions of the total kinetic energy of the fast ejecta–mass-loss rate space excluded by VLA (hatched area) and VLA + XRT (red area) upper limits (see Table 1), as derived assuming the SSA model for a mildly relativistic, nearly isotropic explosion (Sect. 4.1). In addition we show: some peculiar BL-Ic SNe (in green) [1] SN 2002ap (Berger et al. 2002), [2] SN 2010ay (Sanders et al. 2012), [3] SN 2007bg (Salas et al. 2013), [4-5-6] PTF 11cmh - PTF 11qcj - PTF 14dby (Corsi et al. 2016); the relativistic SNe (in blue) [7] SN 2009bb (Soderberg et al. 2010) and [8] SN 2012ap (Chakraborti et al. 2015); [9] SN 2016coi (brown; Terreran et al. 2019); the ll-GRBs (in red) [10] SN 1998bw/GRB 980425 (Li & Chevalier 1999), [11] SN 2006aj/GRB 060218 (Soderberg et al. 2006b) and [12] SN 2010bh/GRB 100316D (Margutti et al. 2013).

sequently, we express $\nu_{m,0}$ as a function of $\dot{M}$ and E from (9):

$$\nu_{m,0} = \left(\frac{p-2}{p-1}\right)^2 \frac{2q}{\pi m_e c} \left(\frac{m_p v_w}{m_e c^2}\right)^2 \left(\frac{2\eta \epsilon_e^5}{r_0^7 \mathfrak{F}_0}\right)^{1/2} \left(\frac{E^{5/2}}{\dot{M}^2}\right) . \tag{14}$$

As a result, $F(t,\nu)$ just depends on $\dot{M}$ and E.

We use a grid of $\dot{M}$ and E values to compare our VLA upper limits (Table 1) with the flux densities derived from (10). In Figure 2 we explore the kinetic energy vs. mass-loss rate parameter space considering the (i) radio upper limits (hatched) and (ii) the radio limits plus the X-ray limits (red), which results in more stringent constraints: $E \lesssim 10^{45}$ erg for $\dot{M} \lesssim 10^{-6}$ $M_\odot$ yr^{-1} and $E \lesssim 10^{46}$ erg for $\dot{M} \lesssim 10^{-4} M_\odot$ yr^{-1}. We end by noting that at these low mass-loss rates the effects of FFA are negligible (e.g. Weiler et al. 1986; Fransson & Björnsson 1998).

4.2. SSA emission from a relativistic GRB-like jet

We generated a grid of radio light-curves powered by synchrotron emission from off-axis relativistic jets using the BOXFIT code (v2; van Eerten et al. 2012), which is based on high-resolution, two-dimensional relativistic hydrodynamical simulations of relativistic jets. All the synthetic light curves were compared to our VLA upper limits (Table 1) to determine the allowed region in the parameter space, using the same procedure as in Coppejans et al. (2018).

The radio emission from an off-axis jet depends on the following physical parameters: (1) isotropic-equivalent total kinetic energy $E_{k,\text{iso}}$; (2) CSM density, either for an ISM-like (n constant) or a wind-like CSM ($\rho_{CSM} = \dot{M}/(4\pi R^2 v_w)$ produced by a constant $\dot{M}$); (3) microphysical shock parameters ϵ_e and ϵ_B; (4) jet opening angle θ_j; (5) observer angle with respect to the jet axis θ_{obs}. We fix the power-law index of the shocked electron energy distribution for a typical value in

the range $p = 2$–3, as derived from GRB afterglow modeling (e.g., Curran et al. 2010; Wang et al. 2015) and we generate a model for a range of $\dot{M}$ for an assumed wind velocity of $v_w = 1000$ km s^{-1}.

We explored a grid of parameters, specifically: 10^{-3} cm$^{-3} \leq n \leq 10^2$ cm^{-3}; 10^{-8} $M_\odot$ yr$^{-1} \leq \dot{M} \leq 10^{-3}$ $M_\odot$ yr^{-1}. Two different jet opening angles were used, which encompass representative measured values for other GRBs: $\theta_j = 5°$ and 30°. We considered three observer angles ($\theta_{\text{obs}} = 30°$, 60°, and 90°) and isotropic-equivalent kinetic energies in the range 10^{50} erg $\leq E_{k,\text{iso}} \leq 10^{55}$ erg. These ranges describe the typical parameters derived from accurate broadband modeling of GRB afterglows (e.g., Schulze et al. 2011; Laskar et al. 2013; Perley et al. 2014; Laskar et al. 2016). Moreover, in this analysis we discuss the results for $\epsilon_e = 0.1$ and $\epsilon_B = 0.01$, but for completeness we show the results for other typical values in Figures 3 and 4. We find that our radio limits are consistent with the expected emission from off-axis ($\theta_{\text{obs}} \geq 60°$) narrow ($\theta_j = 5°$) jets expanding in a low-density CSM environment with $\dot{M} \lesssim 10^{-5}$ $M_\odot$ yr^{-1} that are typical of BL-Ic SNe and GRBs. The allowed beaming-corrected kinetic energy values are $E_k \leq 4 \times 10^{49}$ erg.

5. DISCUSSION

Here we put our results on the environment and on the energetics of SN 2014ad into the broader context of nearby ($z \leq 0.2$) BL-Ic SNe with or without an associated GRB.

5.1. Constraints on uncollimated outflows in SN 2014ad

In the case of sub-relativistic and nearly isotropic ejecta (Sect. 4.1) expanding in a wind-like CSM, assuming equipartition ($\epsilon_e = \epsilon_B = 1/3$), Figure 2 shows that the combination of VLA + XRT data constrains the fast-ejecta kinetic energy to $E \lesssim 10^{45}$ erg for $\dot{M} \lesssim 10^{-6}$ $M_\odot$ yr^{-1} and to $E \lesssim 10^{46}$ erg for $\dot{M} \lesssim 10^{-4} M_\odot$ yr^{-1}. These very deep constraints rule out outflows with properties similar to (i) relativistic SNe, such as SN 2009bb (Soderberg et al. 2010) and SN 2012ap (Chakraborti et al. 2015), for which no GRB counterpart was detected, and (ii) SN 1998bw, a prototypical GRB-SN associated with a low-luminosity GRB, propagating into a similar environment (Figure 2). Our limits also point to very low density environments, consistent with previous findings that BL-Ic SNe favor low-density media (e.g., see Fig. 5 from Margutti et al. 2018), as was also the case for SN 2002ap (Berger et al. 2002) and SN 2010ay (Sanders et al. 2012).

5.2. Is SN 2014ad associated with an off-axis GRB-like jet?

Our VLA radio observations place stringent constraints on off-axis relativistic jets expanding into an ISM-like (Figure 3) and a wind-like CSM (Figure 4), respectively (Sect. 4.2). First, we consider the case of a wind-like CSM and a highly collimated jet with $\theta_j = 5°$ (as is typical for cosmological GRBs) viewed off-axis, for $\epsilon_e = 0.1$ and $\epsilon_B = 0.01$ (top right panel, Figure 4). These off-axis narrow jets are ruled out regardless of the observer angle for $\dot{M} \gtrsim 10^{-5}$ $M_\odot$ yr^{-1} and $E_{k,\text{iso}} \gtrsim 10^{52}$ erg (typical value for a GRB). Hence, GRB-like jets expanding either in a low-density CSM typical of BL-Ic SNe ($\dot{M} \lesssim 10^{-5} - 10^{-6}$ $M_\odot$ yr^{-1} in Table 1 of Smith 2014; see also Li & Chevalier 1999 and Soderberg et al. 2006b) or in typical GRB environments ($10^{-7} \lesssim \dot{M} \lesssim 10^{-5}$ $M_\odot$ yr^{-1}; Laskar et al. 2014, 2015) cannot be ruled out.
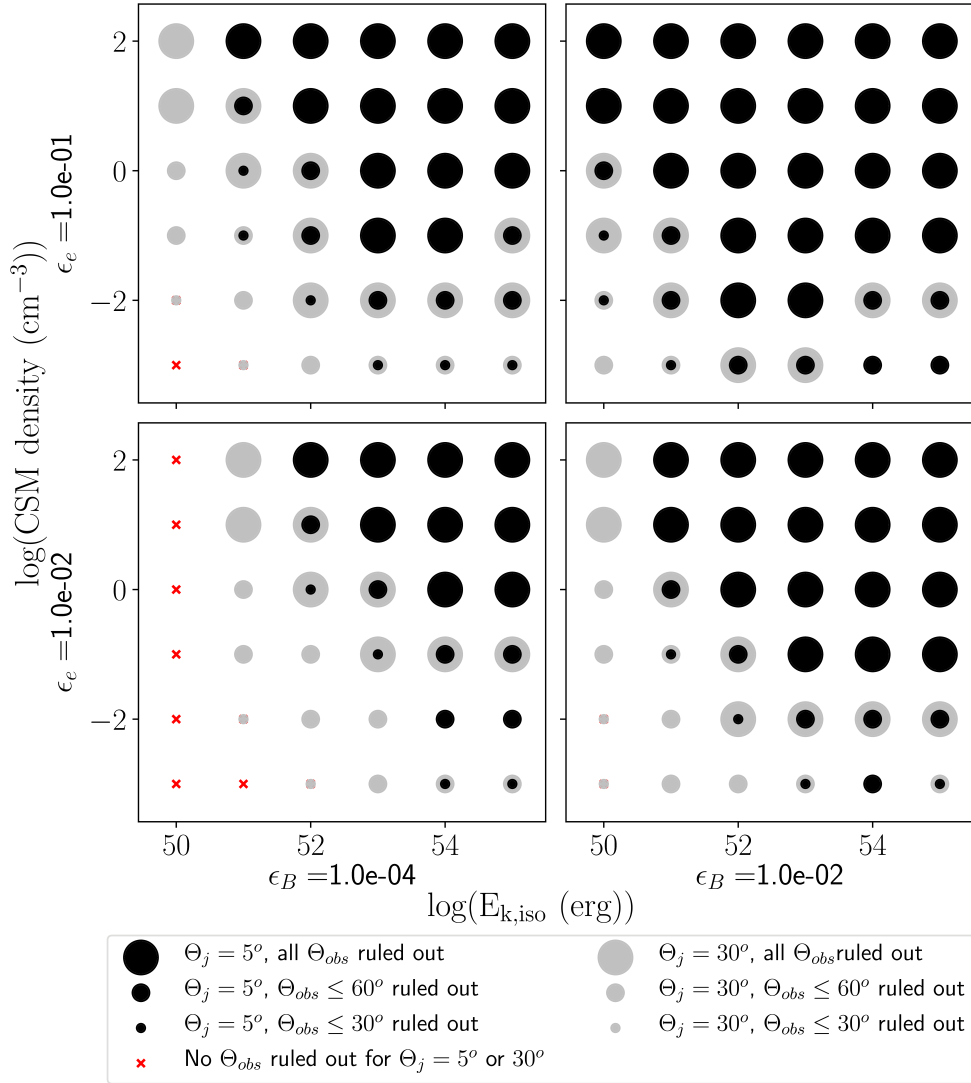
FIG. 3.— Constraints on jetted outflows in an ISM-like density profile in the CSM, based on the VLA upper limits of SN 2014ad and hydrodynamic simulations with BOXFIT(v2) code (Sect. 4.2). Black circles represents jet opening angles of $\theta_j = 5°$, whereas gray circle represents jet opening angles of $\theta_j = 30°$. The symbol size indicates the observer angle (θ_{obs}) out to which we can rule out the corresponding jet, with larger symbols corresponding to larger θ_{obs}. Red crosses indicate that we cannot rule out an off-axis relativistic jet with the given parameters in SN 2014ad. The top (bottom) panels are $\epsilon_e = 0.1$ ($\epsilon_e = 0.01$), and the left (right) panels are $\epsilon_B = 0.0001$ ($\epsilon_B = 0.01$).

In the case of off-axis jets with larger opening angle $\theta_j = 30°$, for $\epsilon_e = 0.1$ and $\epsilon_B = 0.01$ (top right panel, Figure 4), we obtain stronger constraints, due to their larger jet energy. Specifically, regardless of the observer angle, we can rule out scenarios where $\dot{M} \gtrsim 10^{-6}$ $M_\odot$ yr^{-1} and $E_{k,iso} \gtrsim 10^{52}$ erg. Mass-loss rates typically found in the winds of WR stars ($\dot{M} \lesssim 10^{-5} - 10^{-6}$ $M_\odot$ yr^{-1}; Smith 2014) are mostly ruled out. In the case of wide ($\theta_j = 30°$), slightly off-axis ($\theta_{obs} \leq 30°$) jets, for $\epsilon_e = 0.1$ and $\epsilon_B = 0.01$ (top right panel, Figure 4), we can rule out the combination of $\dot{M} \gtrsim 10^{-8}$ $M_\odot$ yr^{-1} and $E_{k,iso} \gtrsim 10^{51}$ erg. Assuming a progenitor wind velocity of 1000 km s^{-1}, all the CSM profiles of all the detected SNe Ibc and most of the GRBs detected to date are rejected (see Figure 5 in Coppejans et al. 2018). We also report the results for a jet propagating into an ISM-like CSM, as the modeling of GRB afterglows often indicates an ISM environment as opposed to a wind-like density profile (e.g., Laskar et al. 2014, 2018). For $\epsilon_e = 0.1$ and $\epsilon_B = 0.01$ (top right panel, Figure 3),

highly collimated jets with $\theta_j = 5°$ are ruled out regardless of the observer angle for $n \gtrsim 10$ cm^{-3} and $E_{k,iso} \gtrsim 10^{50}$ erg, or for $n \gtrsim 10^{-1}$ cm^{-3} and $E_{k,iso} \gtrsim 10^{52}$ erg. A jet with $\theta_j = 30°$ is ruled out for $n \gtrsim 10^{-1}$ cm^{-3} and $E_{k,iso} \gtrsim 10^{50}$ erg. We obtain deeper constraints for jets with $\theta_{obs} < 60°$: for $\theta_j = 5°$ and $\theta_{obs} = 60°$ a jet is ruled out for $n \gtrsim 10^{-3}$ cm^{-3} and $E_{k,iso} \gtrsim 10^{52}$ erg. Hence, GRB-like jets expanding in a ISM-like medium with $n \lesssim 10^{-2}$ cm^{-3} and $E_{k,iso} \lesssim 10^{50}$ erg cannot be ruled out: these densities are compatible with those of some GRBs ($10^{-5} \lesssim n \lesssim 10^3$ cm^{-3}; e.g., Laskar et al. 2014, 2015).

We conclude that we cannot rule out the case of an off-axis ($\theta_{obs} \gtrsim 30°$), narrow ($\theta_j = 5°$) GRB-like jet ploughing through low-density CSM typical of BL-Ic SNe and GRBs; this scenario allows for beaming-corrected kinetic energies $E_{k,iso} \lesssim 10^{52}$ erg in environments sculpted by $\dot{M} \lesssim 10^{-6}$ $M_\odot$ yr^{-1}.
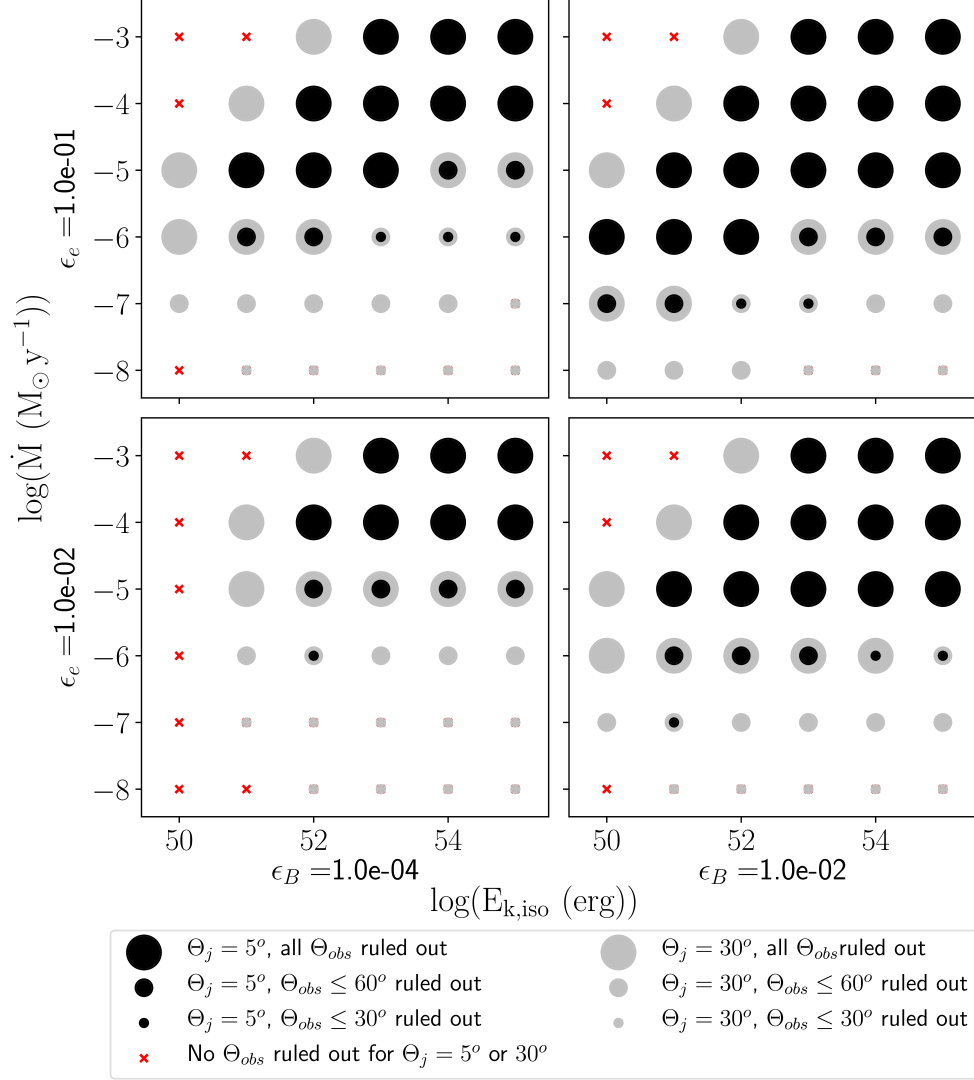
FIG. 4.— Constraints on jetted outflows in a wind-like density profile in the CSM ($\rho \propto r^{-2}$), based on the VLA upper limits of SN 2014ad and hydrodynamic simulations with BOXFIT(v2) code (Sect. 4.2). See the caption of Figure 3 for a full description of the symbols.

5.3. Constraining the $E_k(\Gamma\beta)$ distribution of the ejecta of SN 2014ad

Compared with BL-Ic GRB-less SNe, GRB-SNe seemed to show (i) high mass of ^{56}Ni synthetized in the SN explosion, (ii) higher degree of asphericity in the SN explosion, and (iii) low metallicity of the SN environment (e.g., Cano 2013). However, Taddia et al. (2019) recently showed that the distributions of these observables for the two classes of BL-Ic SNe are still compatible within uncertainties. Another way to investigate the differences between the two classes is offered by the slope x of the kinetic energy profile (E_k) as a function of the ejecta four-velocity ($\Gamma\beta$), parametrized as $E_k \propto (\Gamma\beta)^x$. What is more, this may help to reveal the nature of the explosion (see Fig. 2, Margutti et al. 2014). Steep profiles ($x \lesssim -2.4$) indicate a short-lived central engine, and hence an ordinary Ibc SN (Lazzati et al. 2012); flat profiles ($x \gtrsim -2.4$) indicate the presence of a mildly short-lived central engine, and hence a possible GRB-SN (Margutti et al. 2013); very flat profiles ($x = -0.4$) are typical of ordinary GRBs in the decelerating Blandford-McKee phase (Blandford & McKee

1976), whereas very steep profiles ($x = -5.2$) are characteristic of a pure hydrodynamical spherical explosion (Tan et al. 2001).

For SN 2014ad we explored a grid of parameters in the E_k – $\Gamma\beta$ space. Γ is calculated at $t = 1$ d applying the standard formulation of the fireball dynamics with expansion in a wind-like CSM (e.g., Chevalier & Li 2000)

$$\Gamma_{(t=1\,d)} \sim 18.7 \left(\frac{E_{k,\mathrm{iso}}}{10^{54}erg}\right)^{1/4} \left(\frac{A_*}{0.1}\right)^{-1/4}, \quad (15)$$

where A_* is the circumstellar density, defined with respect to progenitor mass-loss rate $\dot{M}$ and wind velocity v_w as:

$$A_* = \left(\frac{\dot{M}}{10^{-5}M_\odot\,\mathrm{yr}^{-1}}\right)\left(\frac{v_w}{1000\,\mathrm{km\,s}^{-1}}\right). \quad (16)$$

The allowed regions are derived through the conditions described in Sect. 5.2 for the case of a highly collimated jet with $\theta_j = 5°$ (as typical for cosmological GRBs) viewed off-axis in a wind-like CSM (Figure 4; top right panel). Figure 5 shows the allowed region of the beaming-corrected en-
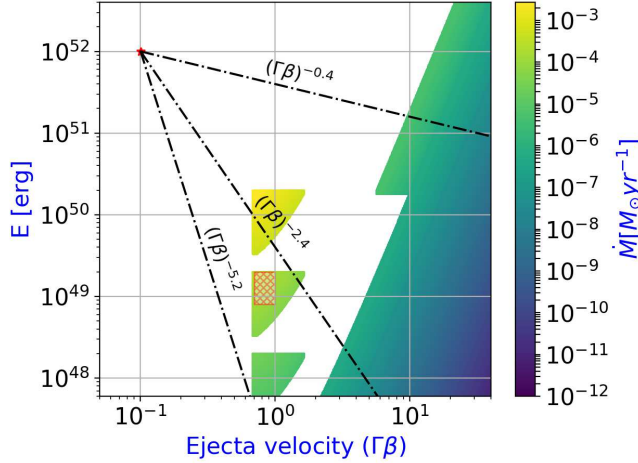
FIG. 5.— Region of the beaming-corrected energy E_k – ejecta velocity $\Gamma\beta$ (with Γ estimated at $t = 1$ d) space allowed by our upper limits of SN 2014ad (in wind-like CSM for relativistic regime). The color scale shows the allowed progenitor mass-loss rate $\dot{M}$. The dashdot lines indicate the slope x of the kinetic energy profile. The orange hatched area indicates the region of relativistic SNe, where the cocoon emission might be observable (De Colle et al. 2018a,b).

ergy E_k – ejecta velocity $\Gamma\beta$ space (in the relativistic regime). Relativistic jets for SN 2014ad are possible for progenitors with very low densities ($\dot{M} \lesssim 10^{-7}$ M$_\odot$ yr^{-1}); for example, a faster-moving ejecta (with a beaming-corrected energy $E_k \sim 10^{51}$ erg) ploughing through a wind-like CSM with a very low density $\dot{M} \sim 10^{-7}$ M$_\odot$ yr^{-1} has $\Gamma\beta \sim 24$ (at $t = 1$ d), compatible with the flat profile ($x = -0.4$) of ordinary GRBs. The lack of any associated GRB suggests a possible off-axis GRB propagating in a wind-like CSM with a very low density ($\dot{M} \lesssim 10^{-7}$ M$_\odot$ yr^{-1}).

5.4. *Constraints on Cocoon emission in SN 2014ad*

The interaction between the jet emission and the outer layers of the progenitor star causes the swelling of the outer envelope of the jet, called cocoon. The recent broadband spectroscopic analysis of Izzo et al. (2019) of a BL-Ic GRB-SN (SN 2017iuk/GRB 171205A) shows the first direct evidence for the cocoon emission. This cocoon is characterized by a very high expansion velocity ($\sim 0.3c$) and probably originates from the energy injection of a mildly-relativistic GRB jet. This discovery could explain the lack of GRBs observed in association with some BL-Ic SNe: the jet, since it transfers a significant part of its total energy to the cocoon, produces the typical GRB emission only if it manages to completely pierce the star photosphere. This conclusion is in agreement with the analysis of De Colle et al. (2018a,b): they show that the radio emission observed in relativistic SNe can be explained as synchrotron emission from the cocoon created by an off-axis GRB jet (either failed or successful), that propagates through the progenitor star. Figure 5 shows the allowed region (red hatched area) for relativistic SNe, where the cocoon emission in principle might be observable: even if the radio emission from SN 2014ad is much fainter than SN 2009bb and SN 2012ap (Figure 1), this region is compatible with E_k of the fast ejecta for a SN 2014ad progenitor with mildly-low densities ($\dot{M} \sim 10^{-5}$ M$_\odot$ yr^{-1}). De Colle et al. (2018a) suggest that, in the off-axis GRB scenario, the cocoon synchrotron emission at radio frequencies dominates (i) always for failed

GRB/cocoon or weak GRB observed off-axis, or (ii) only at early times for energetic off-axis jets with late-times peaks (timescale of years).

A more quantitative discussion of the cocoon emission for SN 2014ad is beyond the scope of the present investigation.

6. CONCLUSIONS

We present deep X-ray and radio limits of the BL-Ic SN 2014ad. Radio and X-ray observations are crucial for probing the fastest moving ejecta in the explosion, as the optical emission is produced by the slow-moving ejecta. Previous studies of this source showed that it has a number of properties that, taken together, suggest a possible GRB counterpart. These include a large bulk energy E_k of the slow ejecta, the asphericity in the explosion and ejecta velocity, the large inferred Nickel mass, and the low progenitor mass-loss rate $\dot{M}$. Consequently, we investigated two different physical scenarios for SN 2014ad: (i) a sub-relativistic, nearly isotropic explosion of an ordinary BL-Ic SN in a wind-like CSM (Sect. 4.1); (ii) an off-axis relativistic jet (Sect. 4.2). These models place strong constraints on the total energy of the fast ejecta (E), the progenitor mass loss rate ($\dot{M}$), the jet opening angle (θ_j) and the observer angle (θ_{obs}). We obtained the following results:

- Assuming that the dominant source of X-ray emission at early times is IC emission from the upscattering of optical photospheric photons into the X-ray band by relativistic electrons at the shock front (Sect. 3), we infer $\dot{M} < 5 \times 10^{-5}$ M$_\odot$ yr^{-1}, for a wind velocity $v_w = 1000$ km s^{-1} for a spherical outflow.

- If SN 2014ad launched a sub-relativistic and isotropic outflow (Sect. 4.1), assuming equipartition ($\epsilon_e = \epsilon_B = 0.33$) we derive limits of $E \lesssim 10^{45}$ erg for $\dot{M} \lesssim 10^{-6}$ M$_\odot$ yr^{-1} and $E \lesssim 10^{46}$ erg for $\dot{M} \lesssim 10^{-4}$ M$_\odot$ yr^{-1}. These deep constraints rule out outflows with properties similar to (i) relativistic SN 2009bb and SN 2012ap, for which no associated GRB was reported, and (ii) SN 1998bw, a prototypical GRB-SN, propagating into a similar environment. E and $\dot{M}$ of the kind seen in the GRB-less SN 2002ap and SN 2010ay, which are characterized by a modest energy budget in the fast ejecta, are not ruled out.

- If SN 2014ad launched a relativistic jet, we (i) rule out collimated on-axis jets of the kind detected in GRBs, (ii) put strong constraints on the energies and CSM densities for an off-axis jet (Figure 3 and 4). We cannot rule out an off-axis GRB in very low-density CSM environments (e.g., $\theta_{obs} \gtrsim 30°$, $\theta_j = 5°$, in a CSM sculpted by $\dot{M} \lesssim 10^{-6}$ M$_\odot$ yr^{-1}, typical of BL-Ic SNe and GRBs). Moreover, we cannot reject the possibility of a radio synchrotron emission dominated by the cocoon created by a GRB jet viewed off axis, that propagates through the stellar progenitor, as expected for relativistic SNe.

With our analysis of the off-axis jet scenario we have demonstrated that it is not possible to rule out off-axis jets expanding into low-density environments (as previously found by Bietenholz 2014 for other SNe). For SN 2014ad we find $\dot{M} \lesssim 10^{-6}$ M$_\odot$ yr^{-1} (Figure 5). If SN 2014ad was indeed powered by an off-axis relativistic jet, our X-ray and radio observations imply extremely low environment densities and energies coupled to jet (unless the jet was far off-axis).

Deep radio and X-ray observations at early and at late times of a large sample of nearby BL-Ic SNe will clarify if relativistic jets are ubiquitous in BL-Ic SNe.

REFERENCES

Berger, E., Kulkarni, S. R., & Chevalier, R. A. 2002, ApJ, 577, L5
Bietenholz, M. F. 2014, PASA, 31, e002
Björnsson, C.-I., & Fransson, C. 2004, ApJ, 605, 823
Blandford, R. D., & McKee, C. F. 1976, Physics of Fluids, 19, 1130
Bromberg, O., Nakar, E., Piran, T., & Sari, R. 2011, ApJ, 740, 100
Burrows, D. N., Hill, J. E., Nousek, J. A., et al. 2005, Space Sci. Rev., 120, 165
Cano, Z. 2013, MNRAS, 434, 1098
Cano, Z., Wang, S.-Q., Dai, Z.-G., & Wu, X.-F. 2017, Advances in Astronomy, 2017, 8929054
Chakraborti, S., Soderberg, A., Chomiuk, L., et al. 2015, ApJ, 805, 187
Chevalier, R. A. 1982, ApJ, 258, 790
Chevalier, R. A. 1996, in Astronomical Society of the Pacific Conference Series, Vol. 93, Radio Emission from the Stars and the Sun, ed. A. R. Taylor & J. M. Paredes, 125
—. 1998, ApJ, 499, 810
Chevalier, R. A., & Fransson, C. 2006, ApJ, 651, 381
Chevalier, R. A., & Li, Z.-Y. 2000, ApJ, 536, 195
Coppejans, D. L., Margutti, R., Guidorzi, C., et al. 2018, ApJ, 856, 56
Corsi, A., Ofek, E. O., Gal-Yam, A., et al. 2014, ApJ, 782, 42
Corsi, A., Gal-Yam, A., Kulkarni, S. R., et al. 2016, ApJ, 830, 42
Cucchiara, A., Levan, A. J., Fox, D. B., et al. 2011, ApJ, 736, 7
Curran, P. A., Evans, P. A., de Pasquale, M., Page, M. J., & van der Horst, A. J. 2010, ApJ, 716, L135
De Colle, F., Kumar, P., & Aguilera-Dena, D. R. 2018a, ApJ, 863, 32
De Colle, F., Lu, W., Kumar, P., Ramirez-Ruiz, E., & Smoot, G. 2018b, MNRAS, 478, 4553
Dessart, L. 2015, in Wolf-Rayet Stars: Proceedings of an International Workshop held in Potsdam, Germany, 1-5 June 2015. Edited by Wolf-Rainer Hamann, Andreas Sander, Helge Todt. Universitätsverlag Potsdam, 2015., p.245-250, ed. W.-R. Hamann, A. Sander, & H. Todt, 245–250
Dessart, L., Hillier, D. J., Woosley, S., et al. 2015, MNRAS, 453, 2189
Dessart, L., John Hillier, D., Yoon, S.-C., Waldman, R., & Livne, E. 2017, A&A, 603, A51
Djorgovski, S. G., Drake, A. J., Mahabal, A. A., et al. 2011, arXiv, arXiv:1102.5004
Eichler, D., & Levinson, A. 1999, ApJ, 521, L117
Eldridge, J. J., Fraser, M., Smartt, S. J., Maund, J. R., & Crockett, R. M. 2013, MNRAS, 436, 774
Ensman, L. M., & Woosley, S. E. 1988, ApJ, 333, 754
Filippenko, A. V. 1997, ARA&A, 35, 309
Fransson, C., & Björnsson, C.-I. 1998, ApJ, 509, 861
Gal-Yam, A. 2017, Observational and Physical Classification of Supernovae, ed. A. W. Alsabti & P. Murdin, 195
Gehrels, N., Chincarini, G., Giommi, P., et al. 2004, ApJ, 611, 1005
Högbom, J. A. 1974, A&AS, 15, 417
Howerton, S., Drake, A. J., Djorgovski, S. G., et al. 2014, CBET, 3831
Izzo, L., de Ugarte Postigo, A., Maeda, K., et al. 2019, Nature, 565, 324
Kalberla, P. M. W., Burton, W. B., Hartmann, D., et al. 2005, A&A, 440, 775
Kellermann, K. I., & Pauliny-Toth, I. I. K. 1981, ARA&A, 19, 373
Kilpatrick, C. D., Takaro, T., Foley, R. J., et al. 2018, MNRAS, 480, 2072
Kulkarni, S. R., Frail, D. A., Wieringa, M. H., et al. 1998, Nature, 395, 663
Laskar, T., Berger, E., Margutti, R., et al. 2015, ApJ, 814, 1
Laskar, T., Berger, E., Zauderer, B. A., et al. 2013, ApJ, 776, 119

Laskar, T., Berger, E., Tanvir, N., et al. 2014, ApJ, 781, 1
Laskar, T., Alexander, K. D., Berger, E., et al. 2016, ApJ, 833, 88
—. 2018, ApJ, 862, 94
Lazzati, D., Morsony, B. J., Blackwell, C. H., & Begelman, M. C. 2012, ApJ, 750, 68
Li, Z.-Y., & Chevalier, R. A. 1999, ApJ, 526, 716
Liang, E., Zhang, B., Virgili, F., & Dai, Z. G. 2007, ApJ, 662, 1111
Margutti, R., Soderberg, A. M., Chomiuk, L., et al. 2012, ApJ, 751, 134
Margutti, R., Soderberg, A. M., Wieringa, M. H., et al. 2013, ApJ, 778, 18
Margutti, R., Milisavljevic, D., Soderberg, A. M., et al. 2014, ApJ, 797, 107
Margutti, R., Chornock, R., Metzger, B. D., et al. 2018, ApJ, 864, 45
Matzner, C. D., & McKee, C. F. 1999, ApJ, 510, 379
Mazzali, P. A., Deng, J., Maeda, K., et al. 2002, ApJ, 572, L61
McMullin, J. P., Waters, B., Schiebel, D., Young, W., & Golap, K. 2007, in Astronomical Society of the Pacific Conference Series, Vol. 376, Astronomical Data Analysis Software and Systems XVI, ed. R. A. Shaw, F. Hill, & D. J. Bell, 127
Modjaz, M., Liu, Y. Q., Bianco, F. B., & Graur, O. 2016, ApJ, 832, 108
Perley, D. A., Cenko, S. B., Corsi, A., et al. 2014, ApJ, 781, 37
Piran, T. 2004, Reviews of Modern Physics, 76, 1143
Podsiadlowski, P., Joss, P. C., & Hsu, J. J. L. 1992, ApJ, 391, 246
Rhoads, J. E. 1999, ApJ, 525, 737
Rybicki, G. B., & Lightman, A. P. 1979, Radiative processes in astrophysics
Sahu, D. K., Anupama, G. C., Chakradhari, N. K., et al. 2018, MNRAS, 475, 2591
Salas, P., Bauer, F. E., Stockdale, C., & Prieto, J. L. 2013, MNRAS, 428, 1207
Sanders, N. E., Soderberg, A. M., Valenti, S., et al. 2012, ApJ, 756, 184
Schulze, S., Klose, S., Björnsson, G., et al. 2011, A&A, 526, A23
Shivvers, I., Modjaz, M., Zheng, W., et al. 2017, PASP, 129, 054201
Smartt, S. J. 2009, ARA&A, 47, 63
—. 2015, PASA, 32, e016
Smith, N. 2014, ARA&A, 52, 487
Soderberg, A. M., Kulkarni, S. R., Berger, E., et al. 2005, ApJ, 621, 908
Soderberg, A. M., Nakar, E., Berger, E., & Kulkarni, S. R. 2006a, ApJ, 638, 930
Soderberg, A. M., Kulkarni, S. R., Nakar, E., et al. 2006b, Nature, 442, 1014
Soderberg, A. M., Chakraborti, S., Pignata, G., et al. 2010, Nature, 463, 513
Stevance, H. F., Maund, J. R., Baade, D., et al. 2017, MNRAS, 469, 1897
Taddia, F., Sollerman, J., Fremling, C., et al. 2019, A&A, 621, A71
Tan, J. C., Matzner, C. D., & McKee, C. F. 2001, ApJ, 551, 946
Terreran, G., Margutti, R., Bersier, D., et al. 2019, arXiv e-prints, arXiv:1905.02226
Van Dyk, S. D., Zheng, W., Brink, T. G., et al. 2018, ApJ, 860, 90
van Eerten, H., van der Horst, A., & MacFadyen, A. 2012, ApJ, 749, 44
Wang, F. Y., Dai, Z. G., Yi, S. X., & Xi, S. Q. 2015, ApJS, 216, 8
Weiler, K. W., Sramek, R. A., Panagia, N., van der Hulst, J. M., & Salvati, M. 1986, ApJ, 301, 790
Yamazaki, R., Yonetoku, D., & Nakamura, T. 2003, ApJ, 594, L79
Yoon, S.-C. 2010, in Astronomical Society of the Pacific Conference Series, Vol. 425, Hot and Cool: Bridging Gaps in Massive Star Evolution, ed. C. Leitherer, P. D. Bennett, P. W. Morris, & J. T. Van Loon, 89